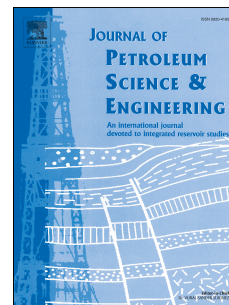


Accepted Manuscript

A non-inertial two-phase model of wax transport in a pipeline during pigging operations

Andrea Boghi, Lloyd Brown, Robert Sawko, Christopher P. Thompson



PII: S0920-4105(18)30184-0

DOI: [10.1016/j.petrol.2018.02.071](https://doi.org/10.1016/j.petrol.2018.02.071)

Reference: PETROL 4741

To appear in: *Journal of Petroleum Science and Engineering*

Received Date: 25 November 2017

Revised Date: 16 February 2018

Accepted Date: 28 February 2018

Please cite this article as: Boghi, A., Brown, L., Sawko, R., Thompson, C.P., A non-inertial two-phase model of wax transport in a pipeline during pigging operations, *Journal of Petroleum Science and Engineering* (2018), doi: 10.1016/j.petrol.2018.02.071.

This is a PDF file of an unedited manuscript that has been accepted for publication. As a service to our customers we are providing this early version of the manuscript. The manuscript will undergo copyediting, typesetting, and review of the resulting proof before it is published in its final form. Please note that during the production process errors may be discovered which could affect the content, and all legal disclaimers that apply to the journal pertain.

A non-inertial two-phase model of wax transport in a pipeline during pigging operations [☆]

Andrea Boghi^{a,*}, Lloyd Brown^b, Robert Sawko^c, Christopher P. Thompson^c

^a*School of Water, Energy and Environment, Cranfield University, Cranfield, Bedfordshire MK43 0AL, UK*

^b*Science Deployed, LLC, Katy, Texas, United States*

^c*IBM Research UK, Hartree Centre, Warrington WA4 4AD, UK*

Abstract

The removal of wax deposit from pipelines is commonly accomplished using pigs. In order to avoid the formation of wax plugs in pipes, bypass pigs, which create a liquid jet to disperse the scraped deposit, are employed. Despite many One-Dimensional (1D) models have been developed to predict the dynamics of bypass pigs, the details of the interaction between the liquid jet and the debris have not been investigated numerically yet. In this work the fluid dynamics of a wax-in-oil slurry in front of a moving bypass pig is studied by means of three-dimensional (3D) numerical simulations. A mathematical model which couples the pig and the wax-in-oil slurry dynamics, solved in the pig frame of reference, has been developed. The results show that the pig quickly reaches an equilibrium velocity, and the pig acceleration is proportional to the square of the mixture relative velocity. Comparing the present with previous sealing-pig results it appears that the bypass flow is more effective in deterring plug formation. Moreover, the 3D fields have the advantage of showing the wax distribution in each pipe section whereas the 1D model cannot distinguish between deposited and suspended wax.

Keywords: bypass pigging, waxy oil, pipe flow, non-inertial frame of

[☆]Modeling wax transport during pigging operations

*A. Boghi

Email address: a.boghi@cranfield.ac.uk (Andrea Boghi)

¹A. Boghi

²L. Brown

³R. Sawko

⁴C. P. Thompson

reference

1. Introduction

Pigging is a common strategy to achieve wax removal in pipelines. The deposited wax is scraped from the walls as the pig is forced along by the oil pressure. Several types of pig can be employed for this procedure, such as the sealing pig, which doesn't allow the passage of fluid through its ends. Many mathematical models have been developed to predict the dynamics of sealing pigs. The pressure drop across the pig is predicted by solving the one-dimensional (1D) mass, momentum and energy conservation equations of the fluids flowing in the pipeline. Besides the pioneering studies (McDonald & Baker, 1964; Barua, 1982), in which the problem is treated in steady state, most of these models investigated the transient flow of gas (Nguyen et al., 2001b,a; Hosseinalipour et al., 2007b; Esmailzadeh et al., 2009) and the two-phase flow of gas and liquid in pipelines (Minami & Shoham, 1995; Lima et al., 1998, 1999; Xu & Gong, 2005; Tolmasquim & Niecele, 2008; Deng et al., 2014). The sealing pig dynamics in complex-shaped pipelines has been also analyzed in a 0D model by Saeidbakhsh et al. (2009).

Despite very useful in pipeline engineering, 1D models do not capture important details of the pig-flow motion. A series of three-dimensional (3D) Computational Fluid Dynamics (CFD) simulations describing the interaction of the waxy oil with a moving sealing pig was presented by Boghi et al. (2017a). The influence of temperature and particle size was discussed.

The main problem of sealing pigs is that the scraped wax accumulates and forms a plug downstream of the pig. If this happens, the oil cannot flow and the pipeline must be shutdown. By introducing a bypass flow this problem can be avoided. This is usually achieved by using a hollow mandrel or by placing holes in the pig seals or discs. The bypass jet transports the removed deposit away from the pig but slows the pig down. The pig velocity can be increased by reducing the bypass section, nevertheless, this reduces the jet strength, and therefore, less material can be suspended in the oil.

Mathematical models, describing the motion of bypass pigs in pipelines, can be found in the literature. Azevedo et al. (1996) developed an algebraic model whose coefficients have been determined through two-dimensional (2D) CFD simulations. One-dimensional modeling of bypass pig in gas pipelines has been extensively used. A model based on the method of characteristics has been developed by Nguyen et al. (2001c) and Nguyen et al. (2001d), and

experimentally verified by Kim et al. (2003). Nieckele et al. (2001) and Hosseinalipour et al. (2007a) solved the system of equations in a moving frame of reference, taking into account the wall deformability. These 1D models use an algebraic expression which relates the pressure drop to the pig velocity.

A semi-empirical model of wax removal using an annular bypass jet has been developed by Southgate (2004) which considered the wax deposit as rigid and part of the pipe wall. The bypass pig dynamics in complex-shaped pipelines has been analyzed in some 0D model, for incompressible (Lesani et al., 2012) and compressible (Mirshamsi & Rafeeyan, 2015) fluids. A good review illustrating the forces acting on a bypass pig in operation was written by Galta (2014).

Despite more than two decades of research, the full 3D flow of the wax-in-oil slurry coupled with the bypass pig dynamics, has not been investigated computationally yet. Three-dimensional numerical simulations have been successfully used to study the flow of the wax-in-oil slurry coupled with the sealing pig (Boghi et al., 2017a). However, that approach is not applicable to the bypass pig case, since: i) the pig velocity and the mean crude-oil velocity are decoupled; ii) the pig and pipe frames of reference are non-inertial.

In this paper a series of 3D CFD simulations describing the interaction of a waxy oil with a moving bypass pig are presented. For this purpose, the model developed in Boghi et al. (2017a) has been modified as follows: i) the pig velocity is calculated by solving the pig momentum equation; ii) the wax-in-oil slurry motion is described in the pig non-inertial frame of reference; iii) the drift-flux model has been modified to include the pig acceleration; iv) the effect of turbulence, due to the oil jet, has been taken into account. The sealing pig study of Boghi et al. (2017a) is referenced to remark the differences with the bypass pig case.

2. Mathematical Modeling

In this section the mathematical model describing the bypass pig dynamics and the wax-in-oil slurry flow in a pipeline is discussed.

2.1. Pig Model

In analogy with Boghi et al. (2017a), the dynamics will be described in a frame of reference fixed to the pig center of mass. This approach has been already used in 1D modeling (Minami & Shoham, 1995; Nieckele et al., 2001;

70 Hosseinalipour et al., 2007b; Tolmasquim & Nieckele, 2008). The conserva-
71 tion of the linear momentum of the pig reads:

$$m_{pig}\vec{a}_{pig} = \int_{A_u} p_m \hat{x} dA - \int_{A_d} p_m \hat{x} dA + \oint_{S_{pig}} \vec{\tau} dA - \vec{F}_d \quad (1)$$

72 where m_{pig} is the pig mass, \vec{a}_{pig} the pig acceleration, p_m is the pressure
73 of the oil-wax mixture, \hat{x} is the axial direction, $\vec{\tau}$ the shear-stress acting on
74 the entire pig surface S_{pig} , A_d, A_u respectively the downstream (head) and
75 the upstream (tail) sides of the pig and \vec{F}_d is the pig-pipe wall friction. The
76 pig velocity \vec{v}_{pig} can be obtained by integrating the acceleration:

$$\vec{v}_{pig}(t) = \int \vec{a}_{pig}(t) dt \quad (2)$$

77 The relationship between the velocity in the absolute frame of reference,
78 \vec{v}_a , and the one in the relative frame of reference, \vec{v} , is

$$\vec{v} = \vec{v}_a - \vec{v}_{pig} \quad (3)$$

79 In the moving frame of reference the pig axial velocity is zero, while in
80 the absolute frame of reference it is equal to $-\vec{v}_{pig}$. Since the pig can move
81 only along the pipe axis, the pig velocity and acceleration and the pig-pipe
82 wall friction can be decomposed as follows: $\vec{v}_{pig} = v_{pig}\hat{x}$; $\vec{a}_{pig} = a_{pig}\hat{x}$; $\vec{F}_d =$
83 $F_d\hat{x}$, where v_{pig}, a_{pig}, F_d are the moduli of respectively the pig velocity, pig
84 acceleration and the pig-pipe wall friction.

85 The pig operation is performed when the wax layer reaches a certain
86 thickness h_w , which is normally much smaller than the pipe diameter. Rep-
87 resenting the wax deposit would require the computational grid thickness to
88 be of the same order of h_w , resulting in a large computational cost. In order
89 to avoid this, the “injection” boundary condition, introduced by Boghi et al.
90 (2017a) has been used. The “injection” boundary condition represents the
91 wax deposit as an “injection area” around the pipe of thickness $h_{inj} > h_w$
92 limiting the computational cost. Boghi et al. (2017a) showed that the flow
93 rate of scraped wax Q_{wax} does not depend on the choice of h_{inj}

$$Q_{wax} = \pi v_{pig} D_{pipe} h_w \left(1 - \frac{h_w}{D_{pipe}} \right) \quad (4)$$

94 where D_{pipe} is the pipe diameter. The pig-wax interfacial area, which is
95 Q_{wax}/v_{pig} , is calculated as the wax removal efficiency was 100%, though in

reality is always smaller. Nevertheless, this approximation is widely used to model the pig-wax deposit contact force (Braga et al., 1999; Barros Jr et al., 2005; Galta, 2014) and it is used here to promote the slurry formation in a short time.

2.2. Fluid dynamic model

The debris field can be considered as a slurry of cut wall wax and oil with variable cut wax content dependent on the wall wax-pig-pipe flow dynamics. In this work, the physical properties of oil and slurry, which are temperature dependent and have been experimentally derived by Boghi et al. (2017a), have been used.

The flow has been simulated with the *drift flux* model, which solves the conservation of mass, momentum and energy of the mixture. In analogy with Boghi et al. (2017a), the inter-phase phenomena, such as settling, have been modeled using the expression proposed by Camenen (2008). The flow has been considered isothermal. This assumption is valid if the observation time is small and is suitable for non-heated pipelines.

Because of the oil jet, there is some turbulent mixing downstream the pig. This has been taken into account using the standard transient $k - \epsilon$ turbulence model. Therefore, all the variables listed below will refer to the mean flow.

The continuity equations for the wax-in-oil slurry is given by:

$$\frac{\partial}{\partial t} (\rho_{wax} \alpha_{wax}) + \text{div} (\rho_{wax} \alpha_{wax} (\vec{v}_m + \vec{v}_{dw})) = 0 \quad (5)$$

where ρ_{wax} is the wax-in oil slurry density, \vec{v}_m is the mixture velocity and \vec{v}_{dw} the drift velocity defined in Boghi et al. (2017a). The mixture momentum equation can be written as:

$$\begin{aligned} \frac{\partial}{\partial t} (\rho_m \vec{v}_m) + \text{div} (\rho_m \vec{v}_m \otimes \vec{v}_m) &= \rho_m (\vec{g} - \vec{a}_{pig}) \\ -\nabla \left(p_m + \frac{2}{3} \rho_m k \right) + \text{div} ([\tau_{dm}] + 2 (\mu_m + \rho_m \nu_T) [S_m]) \end{aligned} \quad (6)$$

where ρ_m is the mixture density, k the turbulent kinetic energy, $[\tau_{dm}]$ the *drift stress tensor*, $\mu_m(T, \alpha_{wax})$ the mixture dynamic viscosity which is a function of both the temperature and the wax volume fraction and $[S_m]$ is

123 the *rate of shear tensor*. The definition of these variables can be found in
124 Boghi et al. (2017a).

125 The turbulent kinematic viscosity ν_T is defined as:

$$\nu_T = C_\mu f_\mu \frac{k^2}{\epsilon} \quad (7)$$

126 where $C_\mu = 0.09$ and f_μ is a wall damping function. The transport
127 equations for k and ϵ are respectively:

$$\begin{aligned} \frac{\partial}{\partial t} (\rho_m k) + \text{div} (\rho_m k \vec{v}_m) &= 2\rho_m \nu_T [S_m] : [S_m] \\ + \text{div} \left(\left(\mu_m + \rho_m \frac{\nu_T}{\sigma_k} \right) \nabla k \right) &- \rho_m \epsilon \end{aligned} \quad (8)$$

$$\begin{aligned} \frac{\partial}{\partial t} (\rho_m \epsilon) + \text{div} (\rho_m \epsilon \vec{v}_m) &= 2C_{\epsilon,1} f_{\epsilon,1} \frac{\epsilon}{k} \rho_m \nu_T [S_m] : [S_m] \\ + \text{div} \left(\left(\mu_m + \rho_m \frac{\nu_T}{\sigma_\epsilon} \right) \nabla \epsilon \right) &- C_{\epsilon,2} f_{\epsilon,2} \rho_m \frac{\epsilon^2}{k} \end{aligned} \quad (9)$$

128 where $\sigma_k = 1, \sigma_\epsilon = 1.3$, are the turbulent Prandtl numbers, $C_{\epsilon,1} =$
129 $1.44, C_{\epsilon,2} = 1.92$, and $f_{\epsilon,1}, f_{\epsilon,2}$ are wall damping functions. In the *drift flux*
130 model the effects of the turbulent small scales coming from the drift-flux
131 terms are considered to be embedded in the turbulent kinematic viscosity, in
132 analogy with Rusche (2003).

133 In order to compare the information given by the 3D fields with the 1D
134 data, we introduce the area fraction of wax-in-oil slurry, defined as:

$$\overline{\alpha_{wax}}(t, x) A(x) = \int_0^{2\pi} \int_0^{R(x)} \alpha_{wax}(t, r, \theta, x) r dr d\theta \quad (10)$$

135 where $R(x)$ is the domain radius, equal to the pipe radius in the pipe
136 domain and to the bypass radius in the pig domain; r is the radial and θ the
137 angular coordinate.

138 Finally, because it is useful for the interpretation of the results, we recall
139 the definition of the Stokes' velocity, which is the terminal velocity of a falling
140 sphere in laminar regime:

$$\vec{v}_s = \frac{1}{18} \frac{(\rho_{wax} - \rho_{oil}) \vec{g} d_{wax}^2}{\mu_{oil}} \quad (11)$$

3. Coupling and Solution Methodology

The mathematical model has been implemented in the **OpenFOAM v3.0** software, which solves the fluid dynamics equations with the Finite Volume Method. The **driftFluxFoam** solver has been modified for this scope. The SIMPLE algorithm has been used for the pressure-velocity coupling.

In this study a general iterative procedure has been implemented to calculate the pig velocity and acceleration. At the first iteration the acceleration is calculated from Eq.(1) using the initial conditions and the pig velocity is calculated from Eq.(2). The pig velocity is used to update the velocity of the pipe walls, which is $-v_{pig}(t)\hat{x}$ in the pig frame of reference, while the pig acceleration is used as a source term in the momentum equation, as shown in Eq.(6). The mixture pressure and the shear stresses are calculated and can be used to update the pig acceleration. The procedure is repeated until either the maximum number of iterations is exceeded or the convergence tolerance is met.

The computational grid has been realized with the **blockMesh** utility of **OpenFOAM v3.0**. The pipe diameter is $3in$ long and the pig is 1 diameter long. These dimensions are not typical of oil pipelines but can be found in test facilities (Barros Jr et al., 2005; Team, 2011; Wang et al., 2015; Huang et al., 2016). The ratio between the pipe and the bypass section is 156.25, which, for continuity reasons, is also the ratio between the bypass and the pipe axial velocity. This requires the usage of a very fine grid in the bypass and reduces considerably the time-step. The domain of investigation is made of the upstream pipe, 2 diameters long, the pig and the downstream pipe which is 60 Diameters long.

The front pig is steady, because of the moving frame of reference, while the pipe wall is sliding backwards at the pig velocity. At the *injection area* only wax is present, with a scraped wax flow rate given by Eq.(4) inwards the pipe. This condition represents the scraping of a 2mm thick wax deposit. The resulting flow rate of scraped wax is about $3.78USgal/min$, regardless of the particle diameter. Therefore, the smaller the particles, the higher their number. Since the injection boundary condition decouples the flow rate of scraped wax from the particle diameter, it is possible to study the influence of these two parameters separately.

As far as the oil and wax volume fraction are concerned, a zero-gradient boundary condition is used everywhere except at the injection area, where a fixed volume fraction is imposed. Eight simulations have been set up. Four

different temperatures, i.e. $-25F, 0F, 25F, 50F$, and 2 particle diameters, i.e. $2mm, 0.4mm$, have been investigated. The uniform particle diameter is an approximation made to study the effect of this parameter. In reality, during the scraping process, particles of different dimensions are injected into the pipe. The temperatures used are very low, and the particle diameters high. Nevertheless, these extreme conditions can be found in the trans Alaska pipeline system (Team, 2011) and have been chosen to provoke crystallization in a short length, and obtain a developed wax-in-oil slurry in a short model time.

4. Results

The simulations have been performed on the Astral Cluster with Xeon 5160 dual core processors at Cranfield University. Each simulation run on 32 processors and took approximately 34 hours and 14 minutes, on a grid made of 232776 hexaedra, to be completed.

The results are presented as function of the temperature and particle diameter. The results with $2mm$ particle diameter are shown first, and secondly those for $0.4mm$ particle diameter. The section average α_{wax} is derived, in order to compare the 3D and 1D results.

In Tab.(1) the properties used for the simulations have been reported. The density and dynamic viscosity values have been experimentally determined and reported in Boghi et al. (2017a). In Tab.(2) the settling velocity is reported for different temperatures and particle diameters.

In order to have meaningful comparisons, the pig velocity should be the same in all the cases studied. Since the physical properties change with the temperature, a different value of the pig-pipe wall friction F_d has been used for the different cases and has been reported in Tab.(1). The F_d has been set in order to have $v_{pig}/U = 0.95$, where $U = Q_{oil}/A$ and Q_{oil} is the oil flow rate.

4.1. Results at $2mm$ wax particle diameter

The pig velocity and acceleration as well as the pressure drop across the pig are reported in Fig.(1). In Fig.(1,a) the time evolution of the pig velocity is shown. At the beginning of the process the pig is at rest. When the oil starts flowing in the pipeline, a pressure drop across the pig is created and the pig accelerates until it reaches an equilibrium velocity. The pig is most effective when it runs at a nearly constant, but not too high, speed (Nguyen

Table 1: Properties used for the simulations

$T(F)$	$\rho_{oil}(g/cm^3)$	$\rho_{wax}(g/cm^3)$	$\mu_{oil}(cP)$	$\mu_{wax}(cP)$	Re_{oil}	$F_d(N)$
-25	0.891	0.98	771.71	7103.6	45	1050
0	0.881	0.98	157.68	3150.5	218	295
25	0.871	0.98	48.92	2026.2	695	160
50	0.861	0.98	20.00	1487.7	1680	115

Table 2: Settling velocity

$T(F)$	$d_{wax}(mm)$	$v_s(mm/s)$
-25	2	-0.251
0	2	-1.369
25	2	-4.857
50	2	-12.97
-25	0.4	-0.010
0	0.4	-0.055
25	0.4	-0.194
50	0.4	-0.519

et al., 2001a; Esmailzadeh et al., 2009; Deng et al., 2014). The higher is the mixture viscosity, the earlier the equilibrium velocity is reached. The pig acceleration and the pressure drop across the pig are plotted against the square of the relative velocity, respectively in Fig.(1,b-c). The direct proportionality between the pressure drop across the pig and the square of the relative velocity and the mixture viscosity is in agreement with the literature (Azevedo et al., 1996; Nguyen et al., 2001c,d; Nieckele et al., 2001; Kim et al., 2003; Hosseinalipour et al., 2007a).

The wax debris field is shown in Fig.(2) at different temperatures. Since the mixture viscosity decreases for the increasing temperature, by virtue of Stokes' law, i.e. Eq.(11), the settling velocity v_s increases with increasing temperature and the wax particles are more dispersed. Overall, by compar-

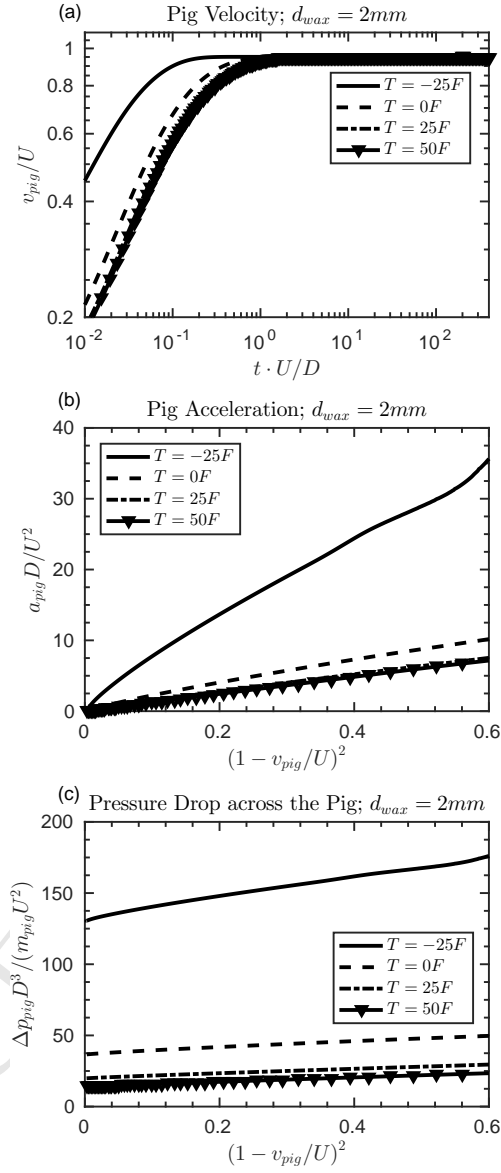


Figure 1: (a) Pig Velocity vs time; (b) Pig Acceleration vs relative velocity; (c) Pressure drop across the pig vs relative velocity. 2mm particle diameter

ing the present results with the sealing pig ones, presented in Boghi et al. (2017a), it can be seen that the bypass improves considerably the wax debris dispersion, not just in proximity of the pig, i.e. 2-4 diameters downstream, but in all the domain investigated, i.e. 60 diameters.

For $T = -25F$ the oil jet penetrates for a distance lower than 1 pipe diameter. The stripped sediment is destroyed and uniformly dissolved in all the domain except at the head of the pig where it is scraped. A similar scenario can be observed for $T = 0F$. The oil jet penetrates for a distance of 4 pipe diameters and the sediment is not destroyed immediately but forms a layer surrounding the oil jet for a diameter. More importantly, at the end of the domain it can be observed a weak stratification with $\alpha_{wax} \simeq 0.35$ at the bottom and $\alpha_{wax} \simeq 0.175$ at the top of the pipe.

The wax debris field appears to be more complex for $T = 25F$ and $T = 50F$. For $T = 25F$ the sediment dissolution is reduced and the stratification becomes more evident. The oil jet penetrates for a distance of 10 diameters. At the top of the oil jet there are two layers: the top one is pure oil while at the top of the jet there are debris with $\alpha_{wax} \simeq 0.7$. Below the jet there is a region at $\alpha_{wax} \simeq 0.5$. A similar distribution of wax particles is present in the entire domain with a region with $\alpha_{wax} \simeq 0.17$ at the center of the pipe. For $T = 50F$ the stratification is more evident with a layer of sediment at the bottom of the pipe. The high wax content region at the top of the jet is longer and thicker. The oil top layer is thicker and the central region is occupied by a slurry with $\alpha_{wax} \simeq 0.5$. Overall, the wax particles are less dispersed compared to lower temperatures, because of the lower mixture viscosity. Nevertheless, confronting the present results with those in Boghi et al. (2017a) the bypass pig is shown to be more effective in dispersing the wax particles.

In Fig.(3) the section averaged wax volume fraction field, defined in Eq.(10), at different instants of time is shown. Regardless of the temperature, the highest wax volume fraction, i.e. $\alpha_{wax} \simeq 0.7$, can be found at the head of the pig, where the wax is scraped. The wax distribution increases slightly in height compared to length. This is in agreement with Boghi et al. (2017a) where it has been concluded that the height of the deposit is set at the beginning of the operations and is a consequence of the local fluid dynamics. Comparing the present results with the sealing pig ones, it can be seen that the wax distribution is more uniform. This confirms the effectiveness of the bypass in dispersing the wax particles. Comparing the 3D field in Fig.(2), with the 1D in Fig.(3,d) it can be seen that, section aver-

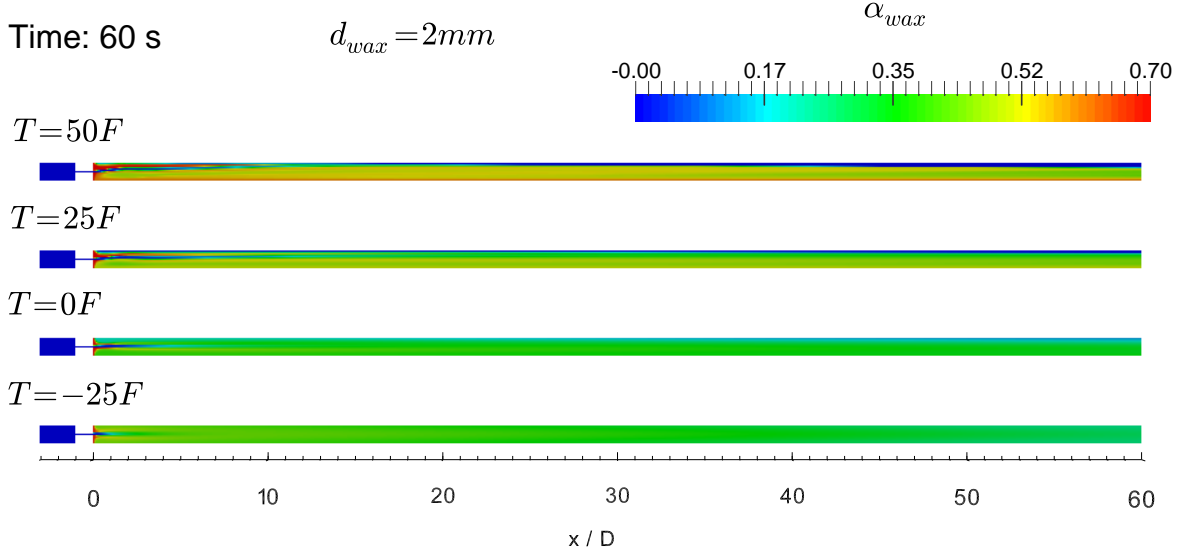


Figure 2: Wax volume fraction field for 2mm particle diameter at 60 seconds after the beginning of the process.

aged is more representative of the instantaneous field when the debris field is dispersed. The stratification which is visible in Fig.(2) for $T = 25F$ and $T = 50F$ cannot be deduced from the section average field.

In Fig.(4) the turbulent kinetic energy in the jet near field is shown for the different temperatures. The results are presented in logarithmic scale to help visualizing turbulence in the jet near field. In a pipe flow, turbulence is generated at the pipe walls and spreads towards the center of the pipe through vortex-shedding. This effect is evident in the bypass because of the higher oil velocity. However, for $T = -25F$, turbulence in the jet is dissipated immediately downstream the bypass because of the high mixture viscosity, reported in Tab.(1), and the highest k is located at the pig head, where the wax is scraped. For $T = 0F$, some turbulence is present in the oil jet ($k \simeq 1m^2/s^2$) but it is dissipated one pipe diameter downstream the bypass ($k \simeq 10^{-3}m^2/s^2$). For $T \geq 25F$ the characteristic turbulent mixing layer at the jet boundary and the potential core region, of triangular shape, at the center of the jet can be observed (Gori et al., 2012; Angelino et al., 2016; Boghi et al., 2016, 2017b). For $T \geq 25F$ the jet bends towards the top of the pipe. This is due to the higher settling.

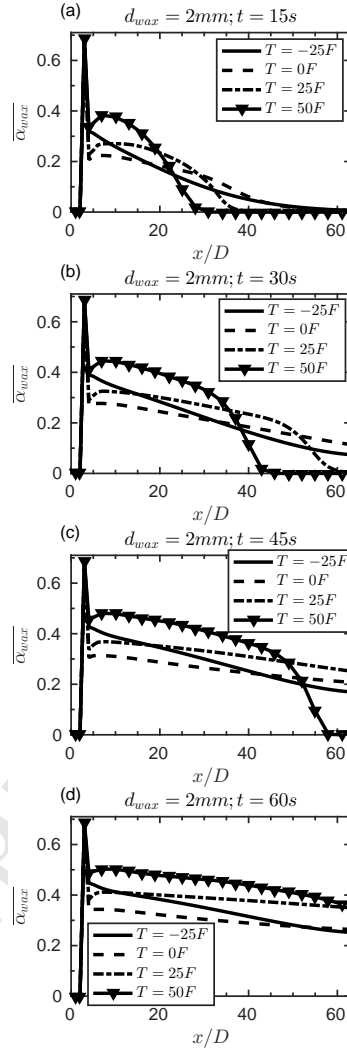


Figure 3: Section averaged wax volume fraction field for 2mm particle diameter. (a) $t = 15s$; (b) $t = 30s$; (c) $t = 45s$; (d) $t = 60s$.

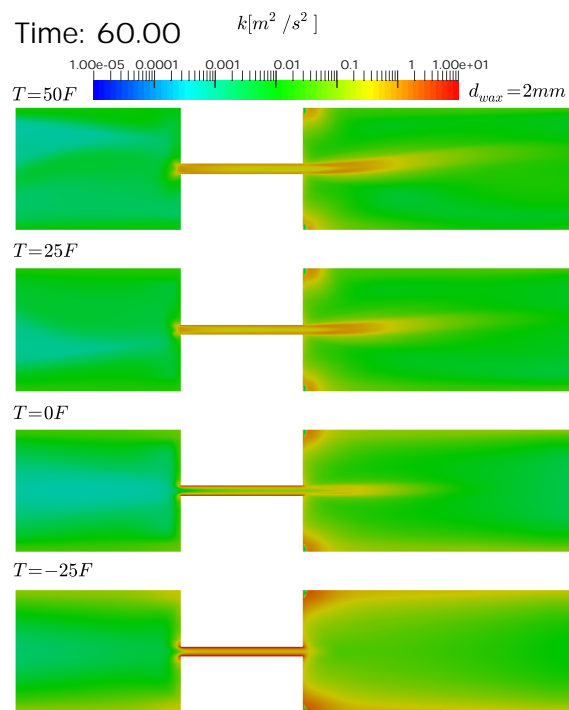


Figure 4: Turbulent kinetic energy field in the near field area of the jet for $2mm$ particle diameter at 60 seconds after the beginning of the process.

281 In Fig.(5,a) we show the mixture axial velocity, scaled by the inlet velocity
 282 U . For every temperature the velocity profile is essentially parabolic. This is
 283 because the section is far from the oil jet where turbulence can be developed,
 284 and because the mixture viscosity is high enough to ensure laminar motion.
 285 For $T = -25F$, $T = 0F$ the profile is almost symmetric because there is
 286 no stratification, whereas for the increasing temperature the highest velocity
 287 moves towards the top where there is pure oil, which has lower mixture
 288 viscosity. The mixture viscosity, scaled by $\rho_m U D$, is shown in Fig.(5,d). As
 289 we can seen from Fig.(5,b) the wax debris for $T = -25F$ is symmetric but not
 290 uniform, as the mixture viscosity. For higher temperatures the stratification
 291 occurs and the mixture viscosity increases towards the bottom. The drift
 292 velocity, shown in Fig.(5,c), is higher at the top of the pipe, because the wax
 293 concentration is lower in this region.

294 4.2. Results at 0.4mm wax particle diameter

295 The results with a wax particle diameter of 0.4mm are discussed in this
 296 section. The temporal evolution of the pig velocity is shown in Fig.(6,a),
 297 while the pig acceleration and the pressure drop across the pig are plotted
 298 against the square of the relative velocity and shown respectively in Fig.(6,b-
 299 c). The results are very similar with those reported in Fig.(1). This is
 300 probably due to the fact that the pig dynamics is mostly influenced by the
 301 pig-pipe wall friction, which does not depend on the particle diameter, and
 302 the pressure drop, which is affected by the settling at the head of the pig but
 303 not at its tail, where there is pure oil. Since the pressure is higher at the
 304 tail of the pig, the particle diameter has a scarce influence in determining
 305 the pig dynamics, at least at the beginning of the process. This parameter
 306 is expected to be important in case of large wax deposit.

307 The wax debris field distribution in the middle section of the pipe, with
 308 a particle diameter of 0.4mm is shown in Fig.(7). Comparing Fig.(2) and
 309 Fig.(7) it can be seen that for $T = -25F$ and $T = 0F$ there is essentially no
 310 difference, except a more uniform field at the end of the domain for $T = 0F$.
 311 The differences are more evident for $T = 25F$ and $T = 50F$. This is due to
 312 the fact that for $T = -25F$ and $T = 0F$ the drift velocity is small enough
 313 to keep the particles in suspension for the duration of the simulation. For
 314 $T = 25F$ and $T = 50F$ the particles appear to be more dispersed. The
 315 oil jet penetrates for approximately the same distance, but it appears to be
 316 straighter, whereas for $d_{wax} = 2mm$ appeared to bend slightly towards the
 317 top, because of the higher deposition. There is no pure oil at the top, but

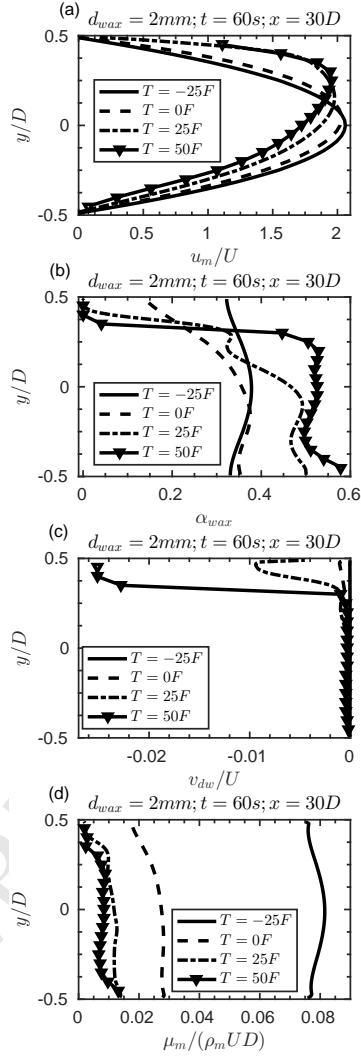


Figure 5: Profiles for $d_{wax} = 2mm$, 60 seconds after the beginning of the process and 30 diameters downstream the FIG. (a) Normalized axial mixture velocity; (b) wax volume fraction; (c) Normalized vertical drift velocity; (d) Normalized Mixture Viscosity.

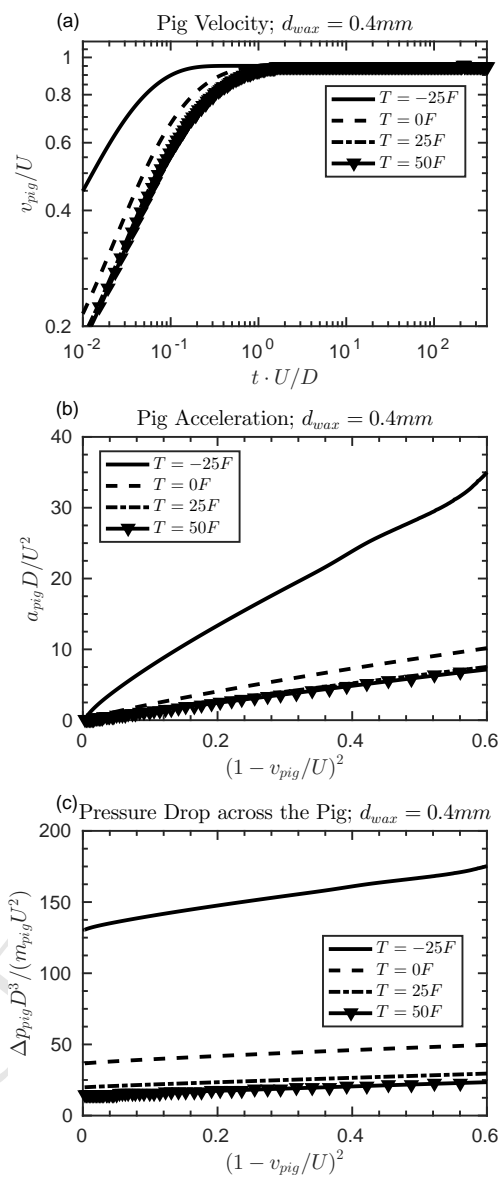


Figure 6: (a) Pig Velocity vs time; (b) Pig Acceleration vs relative velocity; (c) Pressure drop across the Pig vs relative velocity. 0.4mm particle diameter

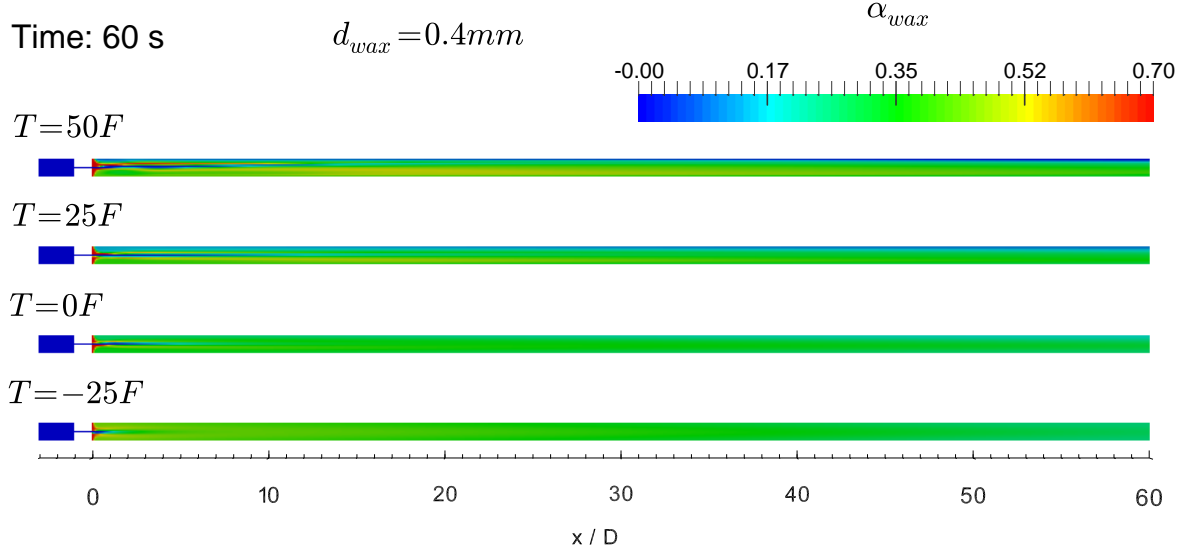


Figure 7: Wax volume fraction field for $0.4mm$ particle diameter at 60 seconds after the beginning of the process.

318 a layer of low wax content. Overall the sediment is destroyed and dispersed
 319 more rapidly compared to the previous and to the sealing pig case in Boghi
 320 et al. (2017a).

321 The section averaged wax debris at different time steps is shown in Fig.(8).
 322 Regardless of the temperature, the highest wax volume fraction, i.e. $\alpha_{wax} \simeq$
 323 0.7, can be found at the head of the pig, where the wax is scraped. In
 324 agreement with the previous results, comparing Fig.(3) with Fig.(8) there is
 325 no visible difference for $T = -25F$ and $T = 0F$. This is due to the reduced
 326 settling velocity, as it can be seen from Tab.(2). For $T = 25F$ and $T = 50F$
 327 instead, it can be seen that the wax distribution is more uniform. The wax
 328 content is lower at the head of the pig and higher at the end of the domain
 329 because of the lower settling velocity which allows the particles to travel
 330 further downstream the pipe. In this case the loss of information between
 331 the 3D and the 1D case is less evident and the volume fraction field in Fig.(7)
 332 is more uniform. Comparing the present results with those in Boghi et al.
 333 (2017a) it can be seen that the section average field is more representative
 334 of the 3D field as well.

335 In Fig.(9) the turbulent kinetic energy in the jet near field is shown for

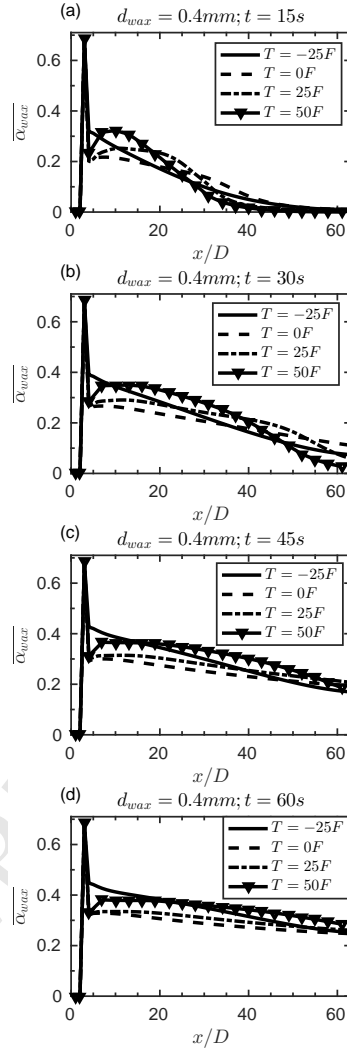


Figure 8: Section averaged wax debris field for 0.4mm particle diameter. (a) $t = 15s$; (b) $t = 30s$; (c) $t = 45s$; (d) $t = 60s$.

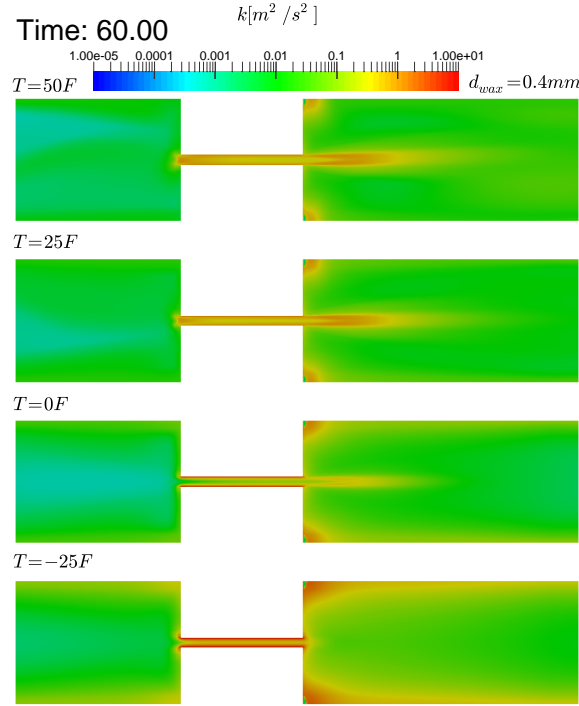


Figure 9: Turbulent kinetic energy field in the near field area of the jet for 0.4mm particle diameter at 60 seconds after the beginning of the process.

the different temperatures. The results are very similar to those already shown in Fig.(9) for the $d_{wax} = 2mm$ case and similar considerations apply. Since the mean oil speed is the same for all temperatures, the jet turbulence is mainly influenced by the mixture viscosity of the wax-in-oil slurry. The higher is μ_m , the lower is k . This effect is amplified by the settling which promotes stratification and removes the wax particles from the jet. Some difference between the two particles diameters investigated can be observed For $T \geq 25F$. In particular, the jet tends to be more straight for $d_{wax} = 0.4mm$, due to the lower settling.

The axial profile of the mixture velocity, scaled by the inlet velocity U , is shown in Fig.(10,a). Comparing the present results with those of Fig.(5,a) it can be seen that the profiles for $T = 25F$ and $T = 50F$ are more symmetric because of the reduced settling velocity, as it can be seen from Tab.(2). The wax volume fraction profile is shown in Fig.(10,b). The wax debris field is never uniform, but has a maximum in the bottom part of the pipe, except

for $T = -25F$ where the debris field distribution is more uniform and the highest wax concentration can be found at the center of the pipe. Comparing Fig.(10,b) with Fig.(5,b) it can be seen that for $T = 25F$ and $T = 50F$ the profiles are more uniform. Similar considerations can be applied for the mixture viscosity profile in Fig.(10,d). The drift velocity instead, Fig.(10,c), is always higher at the top of the pipe, because the wax concentration is lower in this region. Nevertheless, the profiles appear smoother compared to Fig.(5,c).

5. Discussion

The present 3D numerical investigation improves our understanding of bypass pigging and reveals important details which cannot be retrieved from a 1D analysis.

The results show that the oil jet promotes a flow field which is able to keep the debris in suspension not just in the neighborhood of the pig, but in the entire domain investigated, which is 60 diameters long. This is probably due to the high pipe-bypass area ratio, i.e. 156.25, which causes a high speed jet and ensures a high bypass ratio, i.e. $v_{pig}/U \simeq 95\%$. In conclusion the high pipe-bypass area ratio has two advantages: (i) improving the mixing; (ii) making the pig speed almost equal to the inlet oil velocity.

The high speed jet promotes turbulence, which improves debris dispersion. However, this is limited to the jet near field and the velocity profiles appear to be laminar in the far field, as shown in Fig.(5,a) and Fig.(10,a). The laminarization is due to the high mixture viscosity of the wax-in-oil slurry and the low oil flow rate. In a pipeline of wider section the flow in the far field could be transitional or turbulent.

In order to better understand the influence of the jet, the present results should be compared with the sealing pig results (Boghi et al., 2017a), obtained at the same operating conditions. In agreement with Boghi et al. (2017a), the present results show that the temperature has a greater influence on the debris dispersion than the particle diameter. In particular, the lower the temperature and the particle diameter, the more dispersed will be the wax particles distribution, in agreement with Eq.(11). However, the bypass pig appear to be much more effective than the sealing pig in promoting particle suspension.

Since the operating conditions used in the two cases are the same, the higher efficiency of the bypass pig should lie on the flow field promoted by the

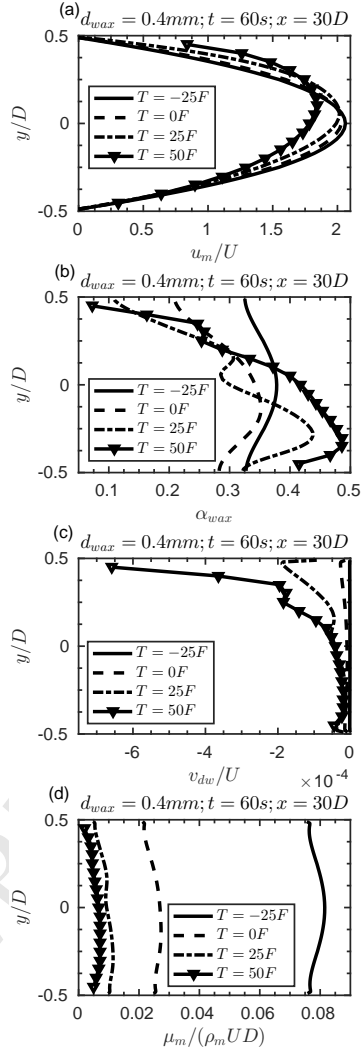


Figure 10: Profiles for $d_{wax} = 0.4mm$, 60 seconds after the beginning of the process and 30 diameters downstream the pig. (a) Normalized axial mixture velocity; (b) wax volume fraction; (c) Normalized vertical drift velocity; (d) Normalized Mixture Viscosity.

jet. In the present study, the velocity at the center of the oil jet is about 300 times higher than the pig velocity. Despite the jet axial velocity diminishes with the increasing distance (Gori et al., 2012; Boghi et al., 2016; Angelino et al., 2016; Boghi et al., 2017b), the acceleration gained in proximity of the pig blasts the wax chips much further downstream compared to the sealing pig. This prevents the deposit from piling up in front of the pig.

The debris field has been predicted using a 3D model. This approach reveals a stratified debris field in case of high settling, e.g. $T = 50F$, $d_{wax} = 2mm$, which cannot be deduced from the 1D results because they only inform the operator on the average wax distribution. A stratified distribution could be inferred by a higher value for the section average wax fraction, but further studies are necessary to test this hypothesis. We can conclude that the 1D information concerning the wax distribution, i.e. Figs.(3,8), is representative of the 3D distribution in Figs.(2,7) when the dispersion is high, because the wax volume fraction profiles are more uniform, as it can be seen from Fig.(5,b) and Fig.(10,b).

6. Conclusions

A 3D numerical investigation of the fluid dynamics of the wax-in-oil slurry during bypass pigging operations has been conducted in this work. The conservation equations have been written in the pig non-inertial frame of reference. The pig dynamics has been taken into account by solving the pig momentum equation and the pig acceleration has been introduced as a momentum source in the momentum equation.

The present numerical results reveal that the bypass improves considerably the wax dispersion compared to the sealing pig (Boghi et al., 2017a), suggesting that the bypass flow is more effective in preventing the deposit from piling up in front of the pig. The 3D simulations give details on the debris distribution which cannot be retrieved from section averaged (1D) results.

The present results have some limitations, as they lack of experimental validation. This was beyond the scope of this work. Nevertheless, the present 3D model is based on the *drift-flux* multiphase model and the standard $k - \epsilon$ turbulence model, which are widely used in scientific research and engineering practice. Therefore the present results can be considered reliable, at least from a qualitative point of view.

7. Acknowledgments

This research did not receive any specific grant from funding agencies in the public, commercial, or not-for-profit sectors.

References

- Angelino, M., Boghi, A., & Gori, F. (2016). Numerical solution of three-dimensional rectangular submerged jets with evidence of the undisturbed region of flow. *Numerical Heat Transfer, Part A: Applications*, 70, 815–830.
- Azevedo, L., Bracm, A., Nieckele, A., Naccxhe, M., Gomes, M. et al. (1996). Simple hydrodynamic models for the prediction of pig motions in pipelines. In *Offshore Technology Conference* (pp. 729–739). Offshore Technology Conference.
- Barros Jr, J., Alves, D., Barroso, A., Souza, R., & Azevedo, L. (2005). Experimental validation of models for predicting wax removal forces in pigging operations. In *Proceedings of 18th International Congress of Mechanical Engineering, Ouro Preto, MG, Brazil* (pp. 6–11).
- Barua, S. (1982). *An Experimental Verification and Modification of the McDonald-Baker Pigging Model for Horizontal Flow*. Ph.D. thesis University of Tulsa, OK.
- Boghi, A., Angelino, M., & Gori, F. (2016). Numerical evidence of an undisturbed region of flow in a turbulent rectangular submerged free jet. *Numerical Heat Transfer, Part A: Applications*, 70, 14 – 29.
- Boghi, A., Brown, L., Sawko, R., & Thompson, C. P. (2017a). An inertial two-phase model of wax transport in a pipeline during pigging operations. *International Journal of Multiphase Flow*, 94, 17–30.
- Boghi, A., Di Venuta, I., & Gori, F. (2017b). Passive scalar diffusion in the near field region of turbulent rectangular submerged free jets. *International Journal of Heat and Mass Transfer*, 112, 1017 – 1031.
- Braga, A., Azevedo, L., & Correa, K. (1999). Resistive force of wax deposits during pigging operations. *Journal of Energy Resources Technology*, 121, 167–171.

- 453 Camenen, B. (2008). Settling velocity of sediments at high concentrations.
454 *Proceedings in Marine Science*, 9, 211–226.
- 455 Deng, T., Gong, J., Zhou, J., Zhang, Y., & Li, H. (2014). Numerical sim-
456 ulation of the effects of vaporization on the motion of pig during pigging
457 process. *Asia-Pacific Journal of Chemical Engineering*, 9, 854–865.
- 458 Esmaeilzadeh, F., Mowla, D., & Asemani, M. (2009). Mathematical modeling
459 and simulation of pigging operation in gas and liquid pipelines. *Journal of*
460 *Petroleum Science and Engineering*, 69, 100–106.
- 461 Galta, T. (2014). *Bypass Pigging of Subsea Pipelines Suffering Wax Depo-*
462 *sition*. Master's thesis Institutt for petroleumsteknologi og anvendt geo-
463 fysikk.
- 464 Gori, F., Angelino, M., Boghi, A., & Petracci, I. (2012). Preliminary nu-
465 merical solutions of the evolution of free jets. In *ASME 2012 International*
466 *Mechanical Engineering Congress and Exposition* (pp. 463–469). American
467 Society of Mechanical Engineers.
- 468 Hosseinalipour, S., Khalili, A. Z., & Salimi, A. (2007a). Numerical simulation
469 of pig motion through gas pipelines. In *16th Australian Fluid Mechanics*
470 *Conference, Goald Coast Australia*. volume 12.
- 471 Hosseinalipour, S., Salimi, A., & Khalili, A. Z. (2007b). Transient flow and
472 pigging operation in gas-liquid two phase pipelines. In *16th Australasian*
473 *Fluid Mechanics Conference Crown Plaza, Gold Coast, Australia* (pp. 976–
474 979).
- 475 Huang, Q., Wang, W., Li, W., Ren, Y., Zhu, F. et al. (2016). A pigging
476 model for wax removal in pipes. In *SPE Annual Technical Conference and*
477 *Exhibition* (pp. 1–11). Society of Petroleum Engineers.
- 478 Kim, D. K., Cho, S. H., Park, S. S., Rho, Y. W., Yoo, H. R., Nguyen, T. T.,
479 & Kim, S. B. (2003). Verification of the theoretical model for analyzing
480 dynamic behavior of the pig from actual pigging. *KSME International*
481 *Journal*, 17, 1349–1357.
- 482 Lesani, M., Rafeeyan, M., & Sohankar, A. (2012). Dynamic analysis of small
483 pig through two and three-dimensional liquid pipeline. *Journal of Applied*
484 *Fluid Mechanics*, 5, 75–83.

- 485 Lima, P., Yeung, H. et al. (1998). Modeling of transient two-phase flow
486 operations and offshore pigging. In *SPE Annual Technical Conference and*
487 *Exhibition, New Orleans, USA*. Society of Petroleum Engineers.
- 488 Lima, P., Yeung, H. et al. (1999). Modeling of pigging operations. In
489 *SPE Annual Technical Conference and Exhibition, Texas, USA*. Society
490 of Petroleum Engineers.
- 491 McDonald, A. E., & Baker, O. (1964). A method of calculating multiphase
492 flow in pipe lines using rubber spheres to control liquid holdup. *Drilling*
493 *and Production Practice*, (pp. 56–68).
- 494 Minami, K., & Shoham, O. (1995). Pigging dynamics in two-phase flow
495 pipelines: Experiment and modeling. *Society of Petroleum Engineers*, 10,
496 225–232.
- 497 Mirshamsi, M., & Rafeeyan, M. (2015). Dynamic analysis of pig through two
498 and three dimensional gas pipeline. *Journal of Applied Fluid Mechanics*,
499 8, 43–54.
- 500 Nguyen, T. T., Kim, D. K., Rho, Y. W., & Kim, S. B. (2001a). Dynamic
501 modeling and its analysis for pig flow through curved section in natural
502 gas pipeline. In *Computational Intelligence in Robotics and Automation,*
503 *2001. Proceedings 2001 IEEE International Symposium on* (pp. 492–497).
504 IEEE.
- 505 Nguyen, T. T., Kim, S. B., Yoo, H. R., & Rho, Y. W. (2001b). Modeling and
506 simulation for pig flow control in natural gas pipeline. *KSME International*
507 *Journal*, 15, 1165–1173.
- 508 Nguyen, T. T., Kim, S. B., Yoo, H. R., & Rho, Y. W. (2001c). Modeling and
509 simulation for pig with bypass flow control in natural gas pipeline. *KSME*
510 *International Journal*, 15, 1302–1310.
- 511 Nguyen, T. T., Yoo, H. R., Rho, Y. W., & Kim, S. B. (2001d). Speed control
512 of pig using bypass flow in natural gas pipeline. In *Industrial Electronics,*
513 *2001. Proceedings. ISIE 2001. IEEE International Symposium on* (pp. 863–
514 868). IEEE volume 2.

- 515 Nieckele, A., Braga, A., & Azevedo, L. (2001). Transient pig motion through
516 gas and liquid pipelines. *Journal of Energy Resources Technology*, 123,
517 260–269.
- 518 Rusche, H. (2003). *Computational Fluid Dynamics of Dispersed Two-Phase*
519 *Flows at High Phase Fractions*. Ph.D. thesis Imperial College London
520 (University of London).
- 521 Saeidbakhsh, M., Rafeeyan, M., & Ziaei-Rad, S. (2009). Dynamic analysis
522 of small pigs in space pipelines. *Oil & Gas Science and Technology-Revue*
523 *de l'IFP*, 64, 155–164.
- 524 Southgate, J. (2004). *Wax Removal Using Pipeline Pigs*. Ph.D. thesis
525 Durham University.
- 526 Team, L. F. S. P. (2011). *Low Flow Impact Study FINAL REPORT*. Tech-
527 nical Report Alyeska Pipeline.
- 528 Tolmasquim, S. T., & Nieckele, A. O. (2008). Design and control of pig oper-
529 ations through pipelines. *Journal of Petroleum Science and Engineering*,
530 62, 102–110.
- 531 Wang, W., Huang, Q., Liu, Y., Sepehrnoori, K. et al. (2015). Experimental
532 study on mechanisms of wax removal during pipeline pigging. In *SPE An-*
533 *nuual Technical Conference and Exhibition* (pp. 1–25). Society of Petroleum
534 Engineers.
- 535 Xu, X.-X., & Gong, J. (2005). Pigging simulation for horizontal gas-
536 condensate pipelines with low-liquid loading. *Journal of Petroleum Science*
537 *and Engineering*, 48, 272–280.

February 16, 2018

To The Editor,
Journal of Petroleum Science and Engineering

Highlights

Title: *A non-inertial two-phase model of wax transport in a pipeline during pigging operations*

1. Bypass pigging in an oil pipeline is studied by means of three-dimensional (3D) numerical simulation;
2. The influence of temperature and particle diameter is studied;
3. A non-inertial solver has been developed;
4. Turbulence has been taken into account;
5. The results of the present 3D numerical investigation reveal the limits of 1D modeling.

Sincerely yours,

Andrea Boghi

Dr. Andrea Boghi,
Senior Research Fellow,
School of Water, Energy and Environment,
Cranfield University,
College Rd,
Cranfield,
Bedford MK43 0AL, UK tel +44 (0)1234 754671,
e-mail : a.boghi@cranfield.ac.uk,